

# Dual impact of global urban overheating on mortality

Received: 31 May 2024

Accepted: 3 March 2025

Published online: 21 April 2025

 Check for updates

Shasha Wang<sup>1</sup>, Wenfeng Zhan<sup>1,2</sup>✉, Bingbing Zhou<sup>3</sup>, Shilu Tong<sup>4,5</sup>,  
TC Chakraborty<sup>6</sup>, Zhihua Wang<sup>7</sup>, Kangning Huang<sup>8</sup>, Huilin Du<sup>1</sup>,  
Ariane Middel<sup>9</sup>, Jiufeng Li<sup>1</sup>, Zihan Liu<sup>10</sup>, Long Li<sup>10</sup>, Fan Huang<sup>11</sup> & Manchun Li<sup>12</sup>

It is known that the urban heat island (UHI) effect could increase mortality in hot seasons, yet its potential health benefits during cold spells are often overlooked. Here we assess the beneficial and detrimental impacts of the UHI effect and associated cooling strategies on temperature-related mortality in more than 3,000 cities worldwide by integrating multi-source datasets. This study finds that the UHI effect reduces global cold-related mortality, surpassing the increase in heat-related mortality more than fourfold. Widely implemented urban cooling strategies, including green and reflective infrastructure, can have an adverse net effect in high-latitude cities but benefit a few tropical cities. We propose seasonal adjustments to roof albedo as an actionable strategy to reduce heat- and cold-related mortality. Our findings highlight that urban heat can protect against mortality in most non-tropical cities in the cold season, emphasizing the importance of seasonally and place-based adaptive UHI mitigation strategies to reduce temperature-related mortality.

The health and well-being of urban populations are central to achieving the Sustainable Development Goals set forth by the United Nations (Sustainable Development Goal (SDG) 11: Sustainable cities and communities)<sup>1</sup>. With Earth's ongoing urbanization and rapid warming, urban overheating has become a major threat to human health, affecting the mortality and morbidity rates in cities globally<sup>2–5</sup>. One of the contributing factors to increased human heat exposure is the urban heat island (UHI) effect, a phenomenon characterized by higher ambient temperatures in cities compared with their rural surroundings<sup>6</sup>. Similar to numerous other anthropogenic environmental and ecological alterations<sup>7</sup>, the UHI effect exhibits a dual impact. It exacerbates heat-related mortality, particularly during periods of increased

temperatures<sup>8–10</sup>, while simultaneously reducing cold-related mortality in cooler conditions<sup>11–14</sup>, as indicated by the broadly recognized 'U-shaped' mortality–temperature relationship curve (Fig. 1). In the context of rapid urbanization and climate change, it is critical to investigate the dual (beneficial and detrimental) impacts of the UHI effect on cold- and heat-related mortality. Understanding this tradeoff will facilitate the context-sensitive design of urban heat mitigation strategies that modify thermal environments appropriately, given the geographic and climatic settings of growing urban populations worldwide<sup>5,15</sup>.

The adverse impacts of the UHI effect on urban energy consumption, economies and human health are well documented<sup>4,13,15,16</sup>. Conversely, several seminal studies have highlighted its potential

<sup>1</sup>Jiangsu Provincial Key Laboratory of Geographic Information Science and Technology, International Institute for Earth System Science, Nanjing University, Nanjing, China. <sup>2</sup>Jiangsu Center for Collaborative Innovation in Geographical Information Resource Development and Application, Nanjing, China. <sup>3</sup>School of International Affairs and Public Administration, Ocean University of China, Qingdao, China. <sup>4</sup>National Institute of Environmental Health Chinese Center for Disease Control and Prevention Beijing, Beijing, China. <sup>5</sup>School of Public Health and Social Work, Queensland University of Technology, Brisbane, Queensland, Australia. <sup>6</sup>Atmospheric, Climate, and Earth Sciences Division, Pacific Northwest National Laboratory, Richland, WA, USA. <sup>7</sup>School of Sustainable Engineering and the Built Environment, Arizona State University, Tempe, AZ, USA. <sup>8</sup>New York University Shanghai, Shanghai, China. <sup>9</sup>Global Institute of Sustainability and Innovation, Arizona State University, Tempe, AZ, USA. <sup>10</sup>School of Artificial Intelligence, Anhui University, Hefei, China. <sup>11</sup>College of Geography and Remote Sensing, Hohai University, Nanjing, China. <sup>12</sup>School of Geography and Ocean Science, Nanjing University, Nanjing, China. ✉e-mail: zhanwenfeng@nju.edu.cn

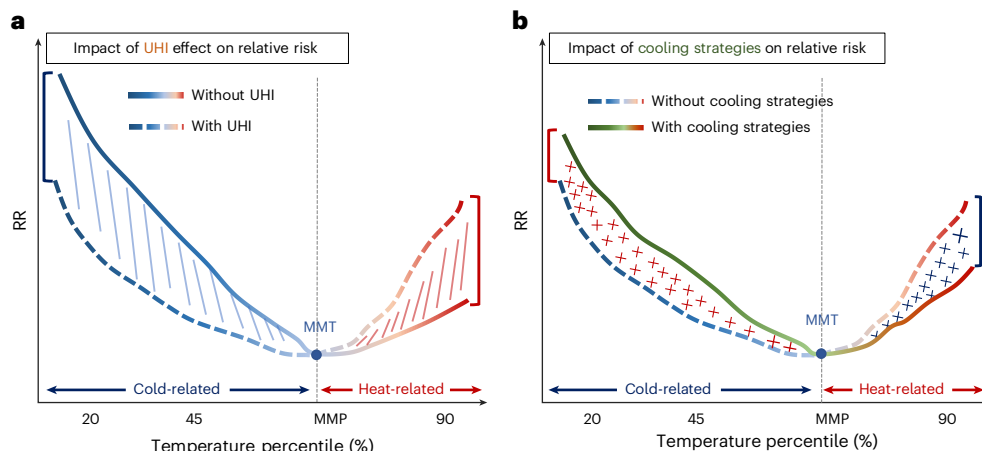


**Fig. 1 | Dual impacts of the UHI effect and heat mitigation strategies on cold- and heat-related mortality relative risk for a hypothetical city.** The annual net impact represents the sum of the beneficial and detrimental impacts. **a**, Curves depicting the relative risk (RR) variation with temperature percentiles in two scenarios: without and with the UHI effect. **b**, Curves depicting the RR changes with temperature percentiles in two scenarios: without (that is, the curve with the UHI effect in **a**) and with urban cooling strategies. The temperature percentile (%) represent the distribution of daily air temperatures. These curves conceptualize the well-established U-shaped relationship between temperature and mortality RR, identifying a MMT ( $^{\circ}\text{C}$ ) and corresponding MMP (%) where RR is the lowest.

Above this MMP/MMT, the city encounters higher heat-related RR, while below it, cold-related RR increases. The UHI effect typically elevates temperatures, exacerbating heat-related RR, while urban cooling strategies reduce these risks. Conversely, below the MMP/MMT, the UHI effect mitigates cold temperatures, but cooling strategies may increase cold-related RR. The diagonally shaded areas and brackets in **a** represent UHI-reduced cold-related RR in temperature intervals below MMT, while denoting UHI-induced heat-related RR in temperature intervals above MMT. The cross-shaded areas and brackets in **b** represent cooling strategies involving increased cold-related RR in temperature intervals below MMT, and decreased heat-related RR in temperature intervals above MMT.

benefits for urban environments<sup>17,18</sup>. However, relatively few studies have examined the dual impact (positive and negative) of the UHI effect on temperature-related mortality<sup>15,19–22</sup>. These studies suggest that the UHI effect is more likely to yield a beneficial annual net effect in higher-latitude cities, but a detrimental effect in cities closer to the Equator<sup>21,22</sup>. Cities in warmer regions typically exhibit a lower minimum mortality percentile (MMP)—defined as the temperature percentile corresponding to the minimum mortality temperature (MMT) where the temperature-related relative risk is minimized. A reduced MMP implies extended exposure to heat stress<sup>5</sup>. Although residents in hotter climates may develop some degree of acclimation, the consequences of sustained and intense heat exposure can still be considerable, exacerbating the detrimental impacts of the UHI effect. By contrast, cities in colder climates may derive benefits from the UHI effect<sup>20</sup>. Theoretically, the dual impact of the UHI effect on annual mortality depends primarily on the MMT (or MMP) and the shape of the mortality–temperature ( $M$ – $T$ ) curve<sup>23</sup> (Fig. 1a), and is indirectly associated with background climate and city-specific socioeconomic and demographic factors<sup>24</sup>. Consequently, the net UHI-induced effects on mortality vary considerably among cities<sup>19</sup>.

Increasing vegetation and adjusting albedo are well-established strategies for mitigating urban heat stress<sup>25–30</sup>. For example, enhancing vegetation has been shown to reduce UHI-induced mortality by 39.5% during summer in European cities<sup>31</sup>. Similarly, increasing albedo can offset approximately 18.0% of UHI-induced heat-related mortality in the West Midlands, UK<sup>32</sup>. Although these interventions may potentially decrease heat-related mortality, they may also increase cold-related mortality by lowering urban temperatures. Although the benefits of these strategies in mitigating heat risk are well documented<sup>26–30</sup>, their adverse impacts on cold-related mortality remain understudied, with only a few case studies available<sup>20,33</sup>. Theoretically, the impact on cold-related mortality depends on the intensity of cooling and effectiveness of regulation—which, therefore, should vary substantially in different urban environments worldwide. Unfortunately, such a global-scale empirical assessment remains lacking, and it hinders the social mobilization of adopting locally and seasonally relevant urban cooling strategies.

Although previous studies have explored the dual impact of the UHI effect on temperature-related mortality under current and projected climate scenarios, these studies have primarily focused on local or regional scales, with a global perspective still lacking. This is mainly owing to the lack of accurate methods for obtaining UHI intensity and establishing city-specific  $M$ – $T$  relationships. Furthermore, the potential adverse consequences of urban cooling strategies on cold-related mortality and annual net mortality across global cities remain under-explored, despite the recognition of their benefits. This knowledge gap would probably be exacerbated by the computational challenges of global numerical simulations in assessing the efficacy of prevalent heat mitigation strategies. Finally, it is unclear whether adaptive strategies exist to optimize benefits in warm periods while minimizing harm during cold seasons.

To address these knowledge gaps, we employed a comprehensive approach that leverages multiple data sources, including remote sensing, climate and socioeconomic data. Utilizing carefully developed computationally efficient data-driven models, we established robust  $M$ – $T$  relationships and quantified the effectiveness of prevalent heat mitigation measures across more than 3,000 cities worldwide. Subsequently, we scrutinized the duality of the UHI effect and assessed the influence of two representative cooling strategies on temperature-related mortality on a global scale. Furthermore, we projected the dual impact of these cooling interventions on future mortality scenarios and proposed novel strategies to mitigate their undesired consequences. Our study offers crucial guidance for formulating effective, context-specific urban heat mitigation policies, thereby improving the well-being of city dwellers and advancing global urban sustainability.

## Impacts of the UHI effect on temperature-related mortality

The dual impact of the UHI effect on annual temperature-related mortality in cities exhibits global variation (Fig. 2 and Supplementary Fig. 1). The reduction in cold-related mortality induced by the UHI effect (51.5%; that is, the summed impacts in all cold days) is 4.4 times greater than the increase in heat-related mortality (11.7%; that

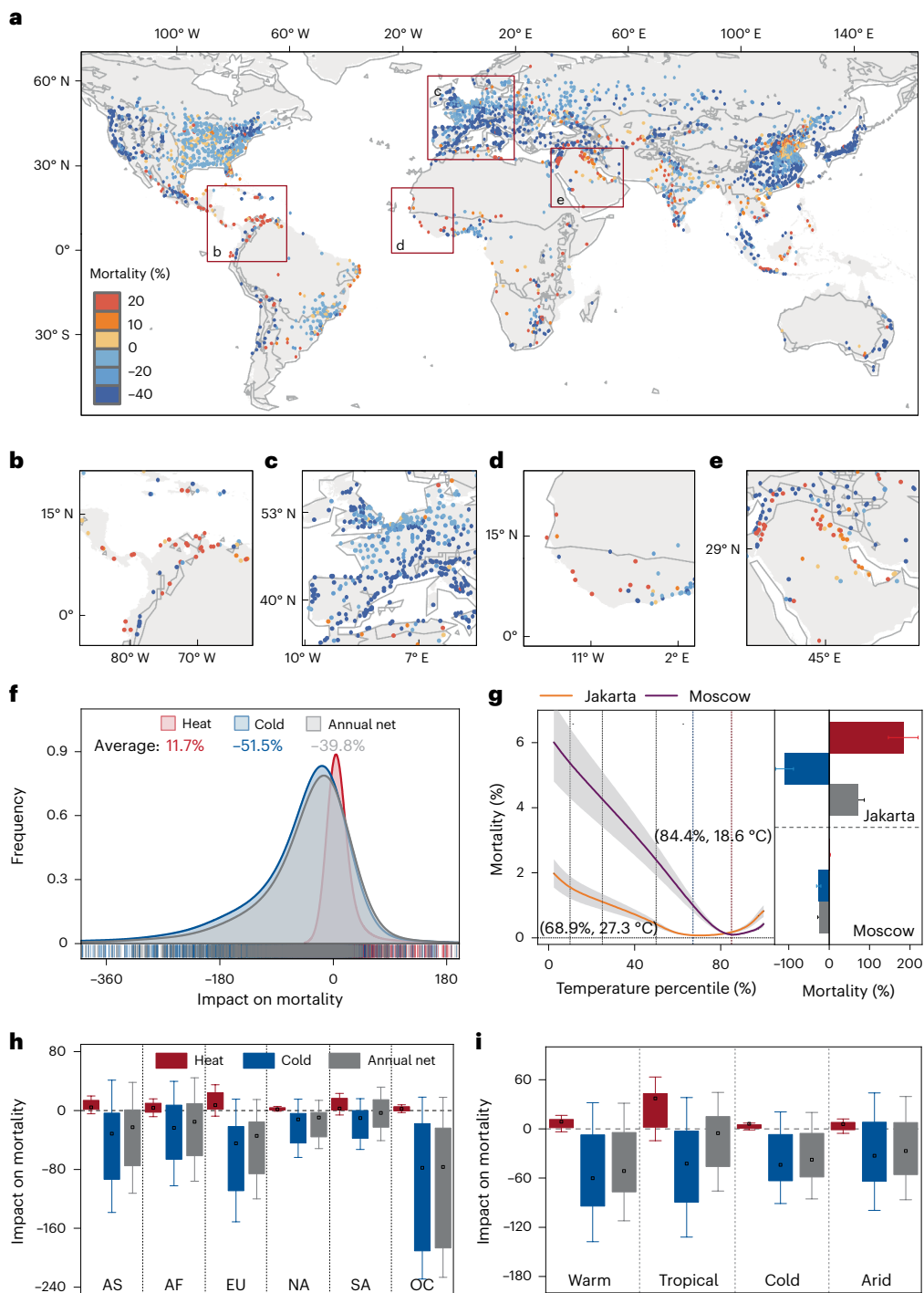


**Fig. 2 | Impacts of the UHI effect on cold- and heat-related mortality in global cities.** **a–e**, Spatial distribution of impacts of the UHI effect on annual net temperature-related mortality in cities worldwide (**a**), Central America (**b**), Europe (**c**), West Africa (**d**) and the Middle East (**e**). **f**, Frequency distribution of impacts of the UHI effect on temperature-related mortality (numbers in the figure denote the average impact). The impacts represent the summed values from the daily attribution, with days above the MMT defined as heat days, and those below MMT as cold days. Notably, a few data points reveal that the UHI effect occasionally exacerbates cold-related mortality and mitigates heat-related mortality, a phenomenon predominantly observed in cities that exhibit an urban cold island effect. **g**, Temperature-related mortality variations for Jakarta and Moscow, fitted using a B-spline function based on four temperature percentile estimates, for illustrative purposes, along with the UHI-induced mortality

(right panel). The shaded area around the curve indicates one standard deviation for all daily attributions within the corresponding temperature interval. Error bars represent one standard deviation of the impacts across all heat days, cold day and an entire year. **h,i**, Impacts of the UHI effect on temperature-related mortality for cities by continent (1,394 Asian cities, 196 African cities, 614 European cities, 841 North American cities, 188 South American cities and 47 Oceanian cities; **h**) and climate zone (1,706 warm cities, 441 tropical cities, 754 cold cities and 379 arid cities; **i**). The small box represents the mean value, with the lower and upper lines indicating the 25th and 75th quantiles, respectively. The whiskers extend to show the outlier range, using an outlier coefficient of 0.5. Positive values indicate an UHI-induced increase in mortality, while negative values denote a reduction. AF, Africa; AS, Asia; EU, Europe; NA, North America; SA, South America; OC, Oceania.

is, the summed impacts in all heat days). This suggests a beneficial annual net impact of the UHI effect on temperature-related mortality (Fig. 2f). Our analysis reveals that the global mean  $M-T$  curve shows a longer exposure period to cold temperatures than to heat, with the global mean MMP reaching 77.9% (Supplementary Fig. 2). Given such a high global mean MMP, the UHI-induced benefits can readily outweigh the harms of temperature-related mortality, resulting in a beneficial effect when considering the entire seasonal cycle globally. Even for some tropical cities (for example, Guangzhou in China) that face higher heat-related risks, the MMPs consistently remain well above 50.0% (Supplementary Fig. 3). For these cities, the high-MMP effect can suppress the substantially larger number of heat than cold days, leading to a beneficial annual net effect (Fig. 2a).

The annual net impacts of the UHI effect on temperature-related mortality differ across climates and continents (Fig. 2a–e). Cities in high-latitude regions are more exposed to cold-related risk and benefit more from the UHI effect. For instance, the reduction in cold-related mortality in Moscow due to the UHI effect is 11.5 times greater than the increase in heat-related mortality (Fig. 2g). By contrast, the net impact of the UHI effect is predominantly detrimental for some low-latitude cities characterized by high heat-related risks. For example, Jakarta in Indonesia exhibits a detrimental annual net mortality effect of 72.4% (Fig. 2g). Regarding cities in different climate zones, the UHI effect has a detrimental annual net effect (Fig. 2i) in some tropical cities (the mean MMP is 65.9%), but it is generally beneficial for other climate cities, especially those in cold climate (the mean MMP is 83.8%; Supplementary Fig. 4). The UHI effect has a substantially beneficial annual net effect on mortality for cities in Europe and Oceania (Fig. 2h). We observe an annual net increase in mortality over several non-tropical cities scattered across mid-to-high latitudes or in arid zones (Fig. 2a). These instances are probably attributable to the presence of urban cool islands over these cities (Supplementary Fig. 5), which manifest in lower urban temperatures relative to the surrounding areas<sup>34</sup>. Urban cool islands may decrease heat-related mortality while potentially increasing cold-related mortality. Furthermore, owing to prolonged exposure to colder temperatures, urban cool islands generally contribute to an overall annual net detrimental impact.

## Effects of cooling strategy on temperature-related mortality

We further examined the dual impacts of two commonly employed urban heat mitigation strategies on temperature-related mortality in cities globally. These strategies include (1) increasing the vegetation fraction by 40%, 30% and 20% of the original fraction in cities with low, medium and high population densities, respectively; and (2) enhancing surface albedo by 40%, 30% and 20% of the original intensity in cities with low, medium and high albedo values, respectively (Methods). In line with previous knowledge, cooling strategies such as increasing vegetation fraction and surface albedo effectively reduce heat-related mortality (Supplementary Figs. 6–8). However, these strategies can also substantially increase cold-related mortality (Supplementary Figs. 7 and 8). A global increase in vegetation can augment cold-related mortality by 6.6%, a rate 5.1 times higher than the reduction in heat-related mortality (Fig. 3e,f). This rate increases to 5.6 when enhancing surface albedo (Fig. 3e,f). These results suggest that these two cooling strategies have a net detrimental effect on global temperature-related mortality annually.

The net impacts of these two cooling strategies on temperature-related mortality show notable spatial differences across regions (Fig. 3). For cities in high-latitude regions, these cooling strategies demonstrate a substantial harmful net effect on annual temperature-related mortality (Fig. 3a–d). The UHI effect typically yields a beneficial net effect annually for such cities (Fig. 2a), but implementing these cooling strategies undermines the protective role of the UHI effect. The net impacts of these cooling strategies on temperature-related mortality

are minimal within the latitude interval around 20° N (Fig. 3c,d). Notably, these strategies are beneficial for some tropical cities, with 17.6% and 16.1% of cities benefiting from the vegetation and albedo strategies, respectively. This demonstrates that the reduction in heat-related mortality attributable to these cooling strategies exceeds the increase in cold-related mortality. Conversely, in other climate zones, this proportion drops below 4% (Fig. 3a,b). The annual net impacts of these two cooling strategies are detrimental across all climate zones and continents (Fig. 3g,h). This effect is particularly pronounced in cities within temperate climate, where there is a 7.7-fold increase in cold-related mortality compared with the reduction in heat-related mortality for the albedo strategy (Fig. 3h), as well as within cold climate, where the increase is 6.0 times (Fig. 3h, and Supplementary Figs. 7 and 8). Among continents, this trend is most pronounced in cities in Oceania (22-fold; Fig. 3g, and Supplementary Figs. 7 and 8).

We further analysed the annual net impacts of urban cooling strategies on temperature-related mortality around 2050 under a moderate emissions pathway (Shared Socioeconomic Pathway (SSP) 2-4.5; Methods). Our analysis demonstrates that implementing these two cooling strategies consistently leads to a global mean increase in cold-related mortality that surpasses the reduction in heat-related mortality (Supplementary Figs. 9 and 10). Notably, the global mean annual net detrimental impact can be further exacerbated by the implementation of more intensive cooling interventions (Supplementary Fig. 9f), even when accounting for future global warming. To reverse this net detrimental impact, we proposed a seasonally adaptive strategy that enhances surface albedo on heat days while reducing it on cold days (Methods). This new seasonally adaptive strategy effectively reduces the negative impact on cold-related mortality associated with the seasonally constant albedo strategy, thereby yielding overall annual benefits (Supplementary Fig. 9b,d and Supplementary Note 1).

## Discussions and implications

We comprehensively assessed the dual impacts of the UHI effect and urban cooling strategies on temperature-related mortality across over 3,000 cities worldwide, considering both current and future scenarios (Figs. 2 and 3, and Supplementary Fig. 9). The assessments demonstrate that our proposed data-driven approach for establishing city-specific  $M-T$  relationships achieves acceptable accuracy (Supplementary Note 2). Importantly, our sensitivity analysis shows that potential uncertainties associated with this data-driven approach have minimal influence on the estimates of UHI-induced annual net mortality, confirming the robustness of our key findings (Supplementary Notes 3–5). A more comprehensive discussion on the robustness and validity of UHI-induced net mortality reduction in global cities is provided in Supplementary Note 6.

## Added value and novelties compared with previous literature

Previous UHI studies have disproportionately centred on hot seasons, during which UHI impacts are net negative<sup>8,27,35,36</sup>. By contrast, our study investigates the dual nature of the UHI effect (Fig. 1), scrutinizing its beneficial and adverse impacts on temperature-related mortality throughout an annual cycle. A few recent studies have acknowledged the dual impact of the UHI effect on temperature-related mortality at a city or regional scale, revealing a detrimental net annual effect, particularly evident in lower-latitude cities<sup>20–22</sup>. What sets our present investigation apart lies in its scope and its delicate inputting of city-specific, context-dependent UHI intensity and mortality–temperature association with satisfactory accuracy. Notably, our study focus is global, involving cities in the global south while incorporating a delicate derivation of UHI intensity and  $M-T$  association through data-mining techniques (Methods).

Our study shows that the UHI effect can yield a net annual benefit even for global south cities, including those in the southern regions of Africa and South America (Fig. 2). In addition, we provide a

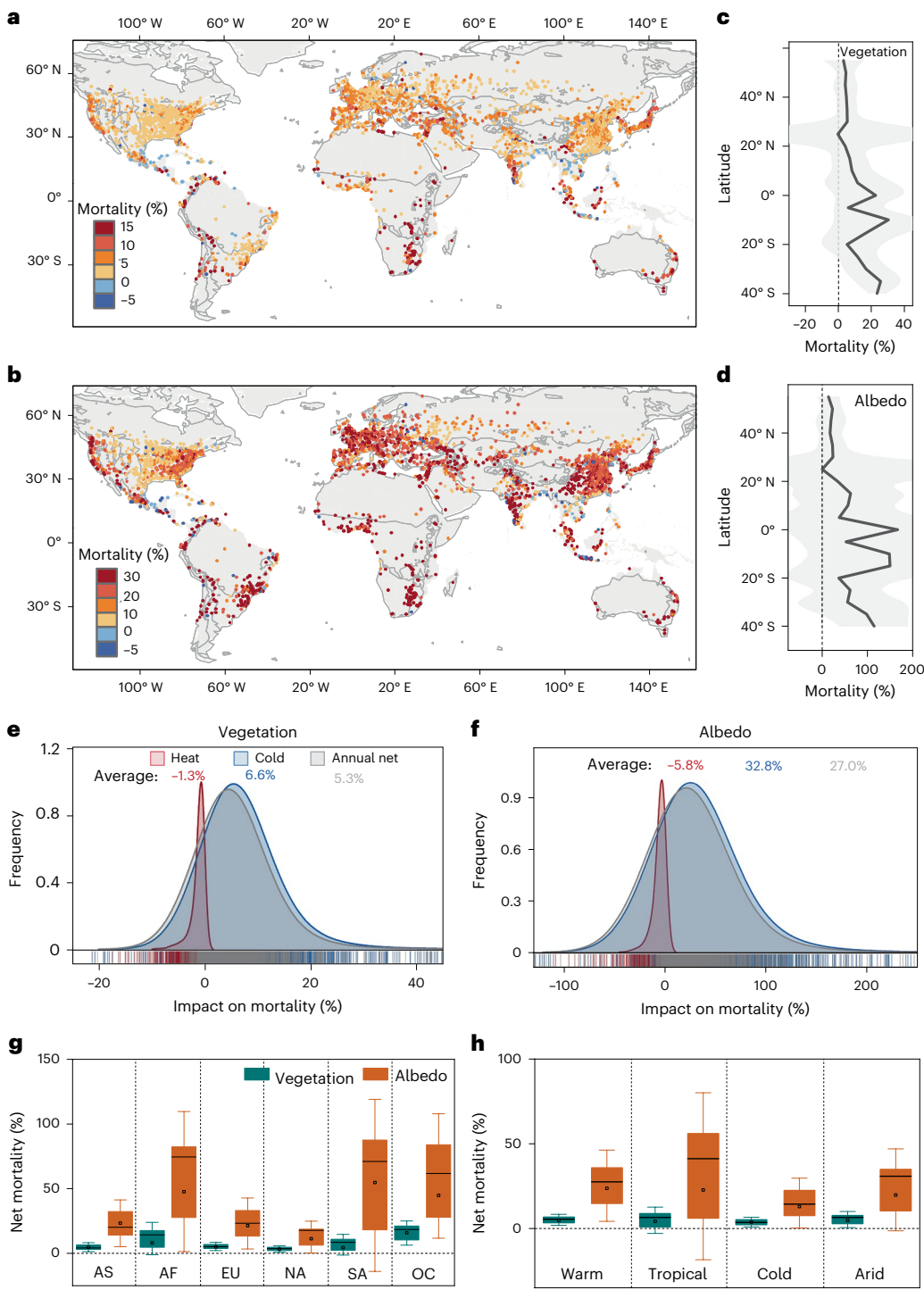


**Fig. 3 | Impacts of urban cooling strategies on cold- and heat-related mortality in global cities.** **a, b**, Spatial distribution of annual net effects on temperature-related mortality with vegetation strategy (a) and albedo strategy (b). **c, d**, Changes in annual net effects depending on latitude with increasing vegetation fraction (c) and surface albedo (d). The shaded areas represent one standard deviation of the impacts of UHI effects on each latitude range. **e, f**, Frequency distribution of effects with increasing vegetation fraction (e) and surface albedo (f; numbers in the figure denote the average impact) on temperature-related mortality. **g, h**, Annual net effects of urban cooling strategies

on temperature-related mortality for cities by continent (1,394 Asian cities, 196 African cities, 614 European cities, 841 North American cities, 188 South American cities and 47 Oceanian cities; **g**) and climate zone (1,706 warm cities, 441 tropical cities, 754 cold cities and 379 arid cities; **h**). The solid line and small box indicate the mean value and median value, respectively. The lower and upper lines of the box indicate the 25th and 75th quantiles, respectively, and the bounds of the whiskers indicate the range of outliers, defined by an outlier coefficient of 0.5. Positive values indicate an increase in mortality due to the implementation of a specific cooling strategy, while negative values indicate the opposite.

comprehensive analysis of the impacts of two common cooling strategies on temperature-related mortality across global cities. These estimates, achieved once more through a cost-effective data-driven approach (Methods), overcome the computational bottlenecks

inherent in numerical simulation methods, thereby quantifying the efficiency of cooling strategies for each city worldwide.

Our study distinguishes itself from prior research by evaluating the net impact of conventional and new seasonally adaptive cooling

strategies on temperature-related mortality. In particular, we account for variations in vulnerability due to economic advancements and aging, which reshape *M-T* associations (Methods). Compared with traditional urban climate studies, which typically assessed UHI-associated mortality using climate-level temperature–RR curves<sup>21</sup>, our research provides a more detailed interpretation of city-specific *M-T* relationships. By contrast to public health studies that predict UHI intensity based on a simple exponential relationship with population growth<sup>14</sup>, we utilize more sophisticated and accurate methods to estimate UHI intensity across global cities. Although studies by Lungman et al.<sup>31</sup> and Huang et al.<sup>19</sup> have made notable contributions by bridging urban climate and public health, their focus remains limited to Europe, whereas our study spans a broader spatial scope and extends across a more extensive temporal horizon by offering future projections (Figs. 2 and 3 and Supplementary Fig. 9).

### Implications and caveats on the design of cooling strategies

Our results show that the UHI effect poses a substantial adverse annual net effect on mortality in some tropical cities. Additionally, an annual net increase in mortality was observed in several non-tropical cities situated at mid-to-high latitudes or in arid zones, mainly due to the presence of urban cool islands (Fig. 2a). This contrasts with the overall beneficial impact observed at the global scale (Fig. 2). UHI-induced detriments on mortality become more prevalent over a considerable portion of cities in Central America (for example, Panama City), nations along the Gulf of Guinea in Africa (for example, Douala, Cameroon) and southern South Asia (for example, Colombo, Sri Lanka). Our findings should not undermine the imperative of implementing urban heat mitigation measures in these cities to address the burden of temperature-related mortality. On the contrary, the urgency of implementing urban cooling strategies becomes even more pronounced for such cities considering the upcoming surface warming trends<sup>37</sup>, augmenting heat exposure due to rapidly growing urban populations<sup>5</sup>, and their high vulnerability to heat stress<sup>38</sup>.

Our results show a global adverse annual net impact on temperature-related mortality by implementing cooling strategies (for example, increasing vegetation fraction and surface albedo; Fig. 3a,b), especially for most mid- and high-latitude cities. For these cities, the conventional cooling strategies weaken the beneficial role of the UHI effect during cold spells, thus amplifying cold-related mortality. These findings show that typical cooling strategies fail to attain their intended objective of reducing temperature-related mortality. Our results reveal that, for such cities, the detrimental impact of conventional urban cooling strategies on cold-related mortality would persistently outweigh their positive effects, even under moderate global warming scenarios extending until at least 2050 (Supplementary Fig. 9). Findings prompt a comprehensive re-evaluation of the benefits of urban cooling strategies in the context of annual net impacts for future applications.

Our findings, which reveal a net negative impact on mortality from increased vegetation in most cities, suggest a preference for deciduous trees over evergreen counterparts. Deciduous trees, reducing evaporative cooling and shade in winter by shedding leaves, can minimize cold-related mortality while preserving cooling benefits and other socio-ecological advantages during the summer<sup>39</sup>. Furthermore, our results indicate the viability of removable and dismountable shading shelters as an effective means for curbing heat-related mortality during the summer while retaining the benefits of the UHI effect in winter<sup>40</sup>. We tested a new seasonal albedo management strategy involving winter-time albedo reduction using adaptable roofing materials that modify albedo in response to sun incident angles or surface temperatures<sup>28</sup>. This strategy aims to alleviate the negative impact on cold-related mortality (Supplementary Fig. 9). Although the concept of albedo reversal holds engineering feasibility<sup>41–43</sup>, its citywide implementation may pose challenges due to potentially high costs and availability of materials. Nevertheless, this strategy could be used at a local scale, particularly over critical areas with high vulnerability, such as

those densely populated by elderly individuals. We must emphasize that comprehensive economic assessments and life cycle analyses remain necessary at various spatial scales to thoroughly analyse the cost-effectiveness of this albedo-reversal strategy<sup>44</sup>.

We need to emphasize that the observed net negative mortality impact associated with increased vegetation in most mid- and high-latitude cities should not be misconstrued as a discouragement against incorporating green infrastructure into urban development or urban renewal initiatives. Mid-latitude cities such as Shanghai, China, Rome, Italy and Phoenix, USA, exemplify instances where urban vegetation is pivotal in reducing urban heat-related mortality via evaporative cooling and shading<sup>45</sup>. Urban green infrastructure facilitates surface cooling and yields multifaceted co-benefits such as ecological enhancements, recreational spaces, health improvements and reduced air pollution<sup>46</sup>. Therefore, urban green infrastructure remains valuable for achieving urban sustainability. Rather than negating the value of green infrastructure, our current study seeks to highlight the duality of the UHI effect, wherein urban heat can function as a protective shield against cold-related mortality, particularly over high-latitude cities in extreme cold events<sup>13,28</sup>. These findings also underline urgent actions to safeguard the public from cold temperatures, a largely underserved aspect in previous studies. Similarly, measures designed to mitigate urban heat during warm seasons may inadvertently negatively impact on temperature-related mortality during cold seasons<sup>28</sup>. The dual nature of cooling strategies warrants careful consideration when introducing any new heat mitigation measures.

### Possible uncertainties and concluding remarks

We acknowledge the inherent uncertainties in assuming linear relationships for vegetation and albedo cooling strategies. Furthermore, our analysis did not fully account for the diversity of vegetation types within cities. Our estimates were based on the assumption of continuous outdoor temperature exposure (Supplementary Note 7), a methodological choice consistent with most epidemiological studies. Additionally, we consistently utilized the air temperature to assess temperature-related mortality<sup>2,5</sup>, and our further comparative analysis using the wet bulb temperature substantiates the reliability of our primary conclusions (Supplementary Note 8). A more detailed discussion of uncertainties and limitations is presented in Supplementary Note 12. Despite these uncertainties, our primary findings remain robust: a prominent dual impact exists in the UHI effect on temperature-related mortality, with the UHI effect serving as an effective shield against mortality during cold periods, particularly for non-tropical cities.

In conclusion, our study seeks to further communicate several critical points by illustrating the global duality of urban heat on mortality: (1) protecting urban dwellers from the cold is equally, if not more, important than protecting them from heat; (2) seasonally adjustable strategies are critical to cool and warm urban surfaces in heat and cold periods respectively, but economic viability is of great importance; and (3) urban policymakers need to consider the escalating heat-related mortality associated with global warming scenarios when designing adaptation measures, as relevant time scales for city adaptation under climate change span decades rather than years.

### Online content

Any methods, additional references, Nature Portfolio reporting summaries, source data, extended data, supplementary information, acknowledgements, peer review information; details of author contributions and competing interests; and statements of data and code availability are available at <https://doi.org/10.1038/s41558-025-02303-3>.

### References

1. United Nations Department of Economic and Social Affairs, Population Division. World Population Prospects 2022: Summary of Results (UN DESA/POP/2022/TR/NO.3, 2022).

2. Kephart, J. L. et al. City-level impact of extreme temperatures and mortality in Latin America. *Nat. Med.* **28**, 1700–1705 (2022).
3. Santamouris, M., Cartalis, C., Synnefa, A. & Kolokotsa, D. On the impact of urban heat island and global warming on the power demand and electricity consumption of buildings – a review. *Energy Build.* **98**, 119–124 (2015).
4. Tong, S., Prior, J., McGregor, G., Shi, X. & Kinney, P. Urban heat: an increasing threat to global health. *Br. Med. J.* **375**, n2467 (2021).
5. Gasparrini, A. et al. Mortality risk attributable to high and low ambient temperature: a multicountry observational study. *Lancet* **386**, 369–375 (2015).
6. Oke, T. R. The energetic basis of the urban heat island. *Q. J. R. Meteorol. Soc.* **108**, 1–24 (1982).
7. Burnside, W. R. et al. Human macroecology: linking pattern and process in big-picture human ecology. *Biol. Rev.* **87**, 194–208 (2012).
8. Laaidi, K. et al. The impact of heat islands on mortality in Paris during the August 2003 heat wave. *Environ. Health Persp.* **120**, 254–259 (2012).
9. Smargiassi, A. et al. Variation of daily warm season mortality as a function of micro-urban heat islands. *J. Epidemiol. Community Health* **63**, 659–664 (2009).
10. Aghamohammadi, N., Ramakrishnan, L., Fong S. C. & Kumar, P. in *Urban Overheating: Heat Mitigation and the Impact on Health* (eds Aghamohammadi, N. & Santamouris, M.) 21–38 (Springer Nature, 2022).
11. Davies, M., Steadman, P. & Oreszczyn, T. Strategies for the modification of the urban climate and the consequent impact on building energy use. *Energy Policy* **36**, 4548–4551 (2008).
12. Chakraborty, T., Hsu, A., Manya, D. & Sheriff, G. A spatially explicit surface urban heat island database for the United States: characterization, uncertainties, and possible applications. *ISPRS J. Photogramm.* **168**, 74–88 (2020).
13. Macintyre, H. L., Heaviside, C., Cai, X. & Phalkey, R. The winter urban heat island: impacts on cold-related mortality in a highly urbanized European region for present and future climate. *Environ. Int.* **154**, 106530 (2021).
14. Zhu, D., Zhou, Q., Liu, M. & Bi, J. Non-optimum temperature-related mortality burden in China: addressing the dual influences of climate change and urban heat islands. *Sci. Total Environ.* **782**, 146760 (2021).
15. Heaviside, C., Macintyre, H. & Vardoulakis, S. The urban heat island: implications for health in a changing environment. *Curr. Environ. Health Rep.* **4**, 296–305 (2017).
16. Li, X. et al. Urban heat island impacts on building energy consumption: a review of approaches and findings. *Energy* **174**, 407–419 (2019).
17. Hirano, Y. & Fujita, T. Evaluation of the impact of the urban heat island on residential and commercial energy consumption in Tokyo. *Energy* **37**, 371–383 (2012).
18. Kolokotroni, M., Zhang, Y. & Watkins, R. The London heat island and building cooling design. *Sol. Energy* **81**, 102–110 (2007).
19. Huang, W. T. K. et al. Assessing the impact of urban heat islands on the risks and costs of temperature-related mortality. In *EGU General Assembly 2023 EGU23-9892* (EGU, 2023).
20. Macintyre, H. L., Heaviside, C., Cai, X. & Phalkey, R. Comparing temperature-related mortality impacts of cool roofs in winter and summer in a highly urbanized European region for present and future climate. *Environ. Int.* **154**, 106606 (2021).
21. Fan, Y. et al. Urban heat island reduces annual building energy consumption and temperature related mortality in severe cold region of China. *Urban Clim.* **45**, 101262 (2022).
22. Lowe, S. A. An energy and mortality impact assessment of the urban heat island in the US. *Environ. Impact Assess.* **56**, 139–144 (2016).
23. Patz, J. A., Engelberg, D. & Last, J. The effects of changing weather on public health. *Annu. Rev. Publ. Health* **21**, 271–307 (2000).
24. Bakhtsiyarava, M. et al. Modification of temperature-related human mortality by area-level socioeconomic and demographic characteristics in Latin American cities. *Soc. Sci. Med.* **317**, 115526 (2023).
25. Hu, K. et al. Modifying temperature-related cardiovascular mortality through green-blue space exposure. *Environ. Sci. Ecotechnol.* **20**, 100408 (2024).
26. Saffari, M. et al. Thermal stress reduction in cool roof membranes using phase change materials (pcm). *Energy Build.* **158**, 1097–1105 (2017).
27. Imran, H. M., Kala, J., Ng, A. W. M. & Muthukumaran, S. Effectiveness of green and cool roofs in mitigating urban heat island effects during a heatwave event in the city of Melbourne in southeast Australia. *J. Clean. Prod.* **197**, 393–405 (2018).
28. Yang, J. & Bou-Zeid, E. Should cities embrace their heat islands as shields from extreme cold? *J. Appl. Meteorol. Climatol.* **57**, 1309–1320 (2018).
29. Krayenhoff, E. S. et al. Cooling hot cities: a systematic and critical review of the numerical modelling literature. *Environ. Res. Lett.* **16**, 053007 (2021).
30. Wang, Z. H. Compound environmental impact of urban mitigation strategies: co-benefits, tradeoffs, and unintended consequence. *Sustain. Cities Soc.* **75**, 103284 (2021).
31. Lungman, T. et al. Cooling cities through urban green infrastructure: a health impact assessment of European cities. *Lancet* **401**, 577–589 (2023).
32. Macintyre, H. L. & Heaviside, C. Potential benefits of cool roofs in reducing heat-related mortality during heatwaves in a European city. *Environ. Int.* **127**, 430–441 (2019).
33. He, C., He, L., Zhang, Y., Kinney, L. P. & Ma, W. Potential impacts of cool and green roofs on temperature-related mortality in the Greater Boston region. *Environ. Res. Lett.* **15**, 094042 (2020).
34. Oke, T. R., Mills, G. & Voogt, J. *Urban Climates* (Cambridge Univ. Press, 2017).
35. Massaro, E. et al. Spatially-optimized urban greening for reduction of population exposure to land surface temperature extremes. *Nat. Commun.* **14**, 2903 (2023).
36. Tan, J. et al. The urban heat island and its impact on heat waves and human health in Shanghai. *Int. J. Biometeorol.* **54**, 75–84 (2010).
37. Liu, Z. et al. Surface warming in global cities is substantially more rapid than in rural background areas. *Commun. Earth Environ.* **3**, 219 (2022).
38. Zhang, H. et al. Unequal urban heat burdens impede climate justice and equity goals. *Innovation* **4**, 100488 (2023).
39. Keeler, B. L. et al. Social-ecological and technological factors moderate the value of urban nature. *Nat. Sustain.* **2**, 29–38 (2019).
40. Turner, V. K., Middel, A. & Vanos, J. K. Shade is an essential solution for hotter cities. *Nature* **619**, 694–697 (2023).
41. Santamouris, M. Using cool pavements as a mitigation strategy to fight urban heat island—a review of the actual developments. *Renew. Sust. Energy Rev.* **26**, 224–240 (2013).
42. Rosso, F. et al. New cool concrete for building envelopes and urban paving: optics-energy and thermal assessment in dynamic conditions. *Energy Build.* **151**, 381–392 (2017).
43. Ramamurthy, P. et al. Influence of subfacet heterogeneity and material properties on the urban surface energy budget. *J. Appl. Meteorol. Clim.* **53**, 2114–2129 (2014).
44. Estrada, F., Botzen, W. W. & Tol, R. S. A global economic assessment of city policies to reduce climate change impacts. *Nat. Clim. Change* **7**, 403–406 (2017).

45. Paschalidis, A., Chakraborty, T., Fatichi, S., Meili, N. & Manoli, G. Urban forests as main regulator of the evaporative cooling effect in cities. *AGU Adv.* **2**, e2020AV000303 (2021).
46. Endrenyi, T. A. Strategically growing the urban forest will improve our world. *Nat. Commun.* **9**, 1160 (2018).

**Publisher's note** Springer Nature remains neutral with regard to jurisdictional claims in published maps and institutional affiliations.

Springer Nature or its licensor (e.g. a society or other partner) holds exclusive rights to this article under a publishing agreement with the author(s) or other rightsholder(s); author self-archiving of the accepted manuscript version of this article is solely governed by the terms of such publishing agreement and applicable law.

© The Author(s), under exclusive licence to Springer Nature Limited 2025

## Methods

### Study area and data

We chose 3,280 cities worldwide, each with an urban area exceeding 30 km<sup>2</sup> in 2018<sup>47</sup>, to investigate the impacts of the UHI effect and urban cooling strategies on annual net temperature-related mortality. These cities span Asia (1,394 cities), Europe (614 cities), North America (841 cities), South America (188 cities), Africa (196 cities) and Oceania (47 cities). Additionally, employing the Köppen–Geiger climate zone<sup>48</sup>, we classified these cities into equatorial (441 cities), arid (379 cities), warm (1,706 cities) and snow cities (754 cities).

The data used include  $M-T$  data, Moderate Resolution Imaging Spectroradiometer (MODIS) data, satellite-based urban surface air temperature (SAT) data, climate data, socioeconomic data and other ancillary data. The city-specific  $M-T$  associations were obtained from refs. 2,5. These results were derived from official mortality records from approximately 700 cities worldwide (Supplementary Fig. 11), meticulously documenting location-specific mortality variations at various temperature percentile ranges (for example, 5%, 10%, 90% and 95%). The  $M-T$  data were utilized to assess the impacts of the UHI effect and associated urban cooling strategies on temperature-related mortality.

The MODIS data consist of the 16-day Enhanced Vegetation Index (EVI; product name: MOD13Q1; 250 m spatial resolution) and the daily albedo estimates (MCD43A3; 500 m). We employed the 2017–2018 EVI and albedo data to portray the spatial distribution of urban vegetation and albedo in cities worldwide, and to assess the impact of urban cooling strategies achieved through increasing the vegetation fraction and surface albedo on temperature-related mortality.

The urban SAT data were obtained from the global near-surface air temperature dataset (1 km spatial resolution) generated based on a series of satellite-derived surface variables and in situ SATs obtained from over 100,000 stations<sup>49</sup>. The generated SAT dataset enhances the description of spatial variations in biophysical and socioeconomic factors affecting temperature<sup>49</sup>, thereby offering a reliable depiction of surface air temperature spatiotemporal patterns. Cross-validations have demonstrated that the generated SATs are highly accurate (with a mean absolute error of 1.49 °C), particularly over impervious surfaces<sup>49</sup>. We employed this dataset to compute UHI intensity, defined as the difference between the mean urban temperature and the mean suburban temperature, rather than absolute temperature values. This subtraction could effectively reduce bias associated with absolute temperature estimations<sup>50</sup>. To derive daily mean values, we averaged the daily maximum and minimum SATs. The mean SAT was used to quantify the canopy-layer UHI intensity, aligning with the daily mean temperature in the  $M-T$  associations.

Our data were obtained from the ERA5-Daily and monthly ERA5-Land reanalysis datasets and the Coupled Model Intercomparison Project Phase 6 (CMIP6) dataset<sup>51,52</sup>. From the ERA5-Daily reanalysis dataset (9 km spatial resolution)<sup>53</sup>, we retrieved the daily mean SAT at 2 m height above ground to represent the daily background air temperature. We retrieved the precipitation, wind speed and radiation data for each city from the monthly ERA5-Land reanalysis dataset. These three climate variables served as background climate inputs for calibrating the impact of urban cooling strategies on urban temperatures. Additionally, from the CMIP6 dataset<sup>51,52</sup>, we retrieved the daily surface air temperature, relative humidity and precipitation in 2050 under a moderate emissions pathway (SSP2-4.5). These data were considered as background climate factors for estimating future UHI intensity.

The socioeconomic data encompass gross domestic product (GDP), the Critical Infrastructure Spatial Index (CISI), the Human Development Index (HDI) and population data. GDP data (2017–2018) were extracted from the global long-term GDP dataset (1 km spatial resolution) generated based on improved nighttime light data<sup>54</sup>. The CISI, with a spatial resolution of 0.1°, quantifies the spatial intensity of urban infrastructure globally, utilizing high-resolution geospatial data from OpenStreetMap for 39 types of critical infrastructure<sup>55</sup>,

such as hospitals. The HDI is a composite index that captures essential aspects of human development—health and longevity, knowledge, and standard of living—derived from a global time-series product with a spatial resolution of 5 arcmin (ref. 56). These indices, along with GDP data, were used as prediction variables to statistically determine the  $M-T$  relationship for each city worldwide. Historical (2017–2018) and future (2050) population data were obtained from the Oak Ridge National Laboratory's LandScan population dataset (<https://landscan.ornl.gov/>)<sup>57</sup> and the projected global population dataset<sup>58</sup>, both at a spatial resolution of 1 km. The population data were used to calculate the urban population for each city. Furthermore, population data for different age groups in various countries and territories were obtained from the United Nations<sup>1</sup> to gather population structure information. This information was then assigned to cities within each territory to quantify the proportion of the population aged over 65. The assigned proportion was used as an age structure factor for statistically establishing the  $M-T$  relationship<sup>39</sup>.

The auxiliary data include the global urban boundary (GUB), elevation and land cover type data. We used the 2018 GUB data<sup>47</sup> to delineate urban and rural areas to calculate the UHI intensity. The elevation data were derived from the GTOPO30 dataset (1 km) provided by the US Geological Survey's Center for Earth Resources Observation and Science (<http://lpdaac.usgs.gov>)<sup>60</sup>. The elevation data were used as a topographic factor in deriving the statistical  $M-T$  relationship and were used to assess the impacts of cooling strategies on urban temperatures. The land cover type data were sourced from the MODIS MCD12Q1 product (500 m spatial resolution). They were used to remove pixels labelled as water bodies, snow and ice, and permanent wetlands<sup>61</sup> to reduce uncertainties in calculating UHI intensity.

### Assessing impacts of the UHI effect on temperature-related mortality

The  $M-T$  profile typically follows a U-shaped curve<sup>62–65</sup>. In such scenarios, the UHI effect exacerbates heat-related mortality on hot days while reducing cold-related mortality on cold days (Fig. 1). Our assessment of the UHI-induced annual net impact on temperature-related mortality complied with the following three steps (Supplementary Fig. 12). First, we calculated the SAT-based UHI intensity for global cities. Second, we estimated the parameters of the  $M-T$  curve for each city. Third, we comprehensively assessed the annual net impact of the UHI effect on temperature-related mortality in cities worldwide.

**Calculating SAT-based UHI intensity globally.** The UHI effect, a distinct local climate phenomenon, manifests as greater temperatures in urban areas compared with suburban areas due to urbanization<sup>6</sup>. Contrastingly, an urban cold island effect occurs instead in a minority of cities, primarily arid cities<sup>66</sup>. These effects are commonly measured by the average temperature difference between the urban and suburban areas<sup>67</sup>. In our study, urban surfaces were delineated using urban areas identified from the 2018 GUB data, while rural surfaces were defined as the areas within the 10-km to 50-km buffers surrounding the urban areas<sup>68</sup>. To minimize uncertainties associated with specific land cover types like 'ice', 'snow', 'water' and 'permanent wetland', corresponding pixels were excluded from urban and rural surfaces when calculating UHI intensity<sup>69</sup>. We then computed the UHI intensity as the average SAT difference between these defined urban and rural surfaces on a monthly basis for global cities (Supplementary Fig. 5).

**Quantifying the  $M-T$  association globally.** Previous studies indicate that the  $M-T$  association is best quantified by considering temperature percentile rather than absolute temperature<sup>70,71</sup>. Two distinct features characterize this association: the MMT and the U-shaped  $M-T$  curve. MMT represents the optimum temperature at which the minimum mortality occurs, while the MMP denotes the percentile of MMT (Fig. 1). Urban populations face heat-related mortality risks when the daily

temperature exceeds MMT. At the same time, cold-related mortality risks arise when the daily temperature is lower than MMT<sup>62</sup>. The values of MMT and the U-shaped *M-T* curve differ depending on the cities' background climate and socioeconomic conditions<sup>24</sup>. Obtaining information on MMT and the U-shaped *M-T* curve can often be challenging, if impossible, especially for most cities in developing and underdeveloped nations. This is primarily owing to the heavy reliance on comprehensive and detailed official mortality records documented in hospitals and medical centres to ascertain MMT and the U-shaped *M-T* curve.

We developed a machine learning method to acquire each city's MMT and U-shaped data using *M-T* information from a constrained set of cities<sup>72</sup>. Our investigation sourced comprehensive *M-T* curves from approximately 700 cities worldwide, meticulously extracted from official mortality records<sup>2,5</sup>. This set of cities encapsulates diverse background climates and socioeconomic contexts by encompassing 19 nations (Supplementary Fig. 11), including the USA, Canada, the UK, Italy, Spain, Sweden, China, Japan, South Korea, Thailand, Australia, Brazil, Argentina, Chile, Mexico, Peru, Costa Rica, El Salvador and Guatemala. This set of cities offers intricate data concerning MMT and the U-shape at different temperature percentiles (for example, 5%, 10%, 50%, 90% and 95%). We uniformly integrated these mortality percentiles into four categories (that is, >5%, 5%–MMT, MMT–95% and >95%), representing mortality variations from extreme cold, non-extreme cold, non-extreme heat to extreme heat, respectively. We trained a random forest model to establish a statistical relationship between dependent variables (that is, the MMT and mortality at four percentiles) and a range of climatic, socioeconomic and urban infrastructure factors. These factors encompassed SAT, dew point temperature, precipitation, wind speed, altitude, latitude/longitude, GDP, population structure (the proportion of population aged over 65)<sup>59</sup>, CISI and HDI. The rationale for selecting these indicators is elaborated in Supplementary Note 10. The random forest model was trained using data from the above-noted cities and then applied to infer the MMT (Supplementary Fig. 3) and mortality at different temperature percentiles for over 3,000 cities worldwide. Additionally, we estimated the MMPs using a similar approach to illustrate the relationship between mortality and temperature percentile (Supplementary Fig. 3). This characterization is intended to facilitate an intuitive understanding of the discrepancies in temperature-related mortality across cities.

On this basis, we utilized global daily air temperature data to quantify temperature intensity values across various temperature percentiles for each city. Based on the established U- or V-shaped mortality–temperature relationship<sup>2,62,71</sup>, we derived the specific correlations between temperature and mortality within each temperature percentile interval. This derivation allowed us to quantify the increase in heat-related mortality or the decrease in cold-related mortality for each 1 °C rise in temperature<sup>2</sup>. Using this relationship with daily air temperature data, we estimated the daily temperature-related mortality for each city under any given day of various temperature conditions. By summing daily mortality and categorizing days with temperatures above the MMT as heat days and below as cold days, we then calculated city-specific cold-related and heat-related mortality. The detailed procedures are provided in Supplementary Fig. 13.

**Assessing the impact of the UHI effect on annual net mortality.** To examine the UHI impact on cold- and heat-related mortality, we categorized each city's months as cold or warm based on global MMT estimates (Supplementary Fig. 3). Months with temperatures above the MMT were classified as warm, and those below as cold. We then calculated the UHI values for the cold and warm seasons by averaging the UHI intensity across the respective months. Based on the mortality–temperature relationship (that is, increased heat-related mortality or decreased cold-related mortality per 1 °C rise), we quantified the temperature-related mortality by simultaneously considering

background temperature and UHI. The impact of the UHI effect was distinguished by comparing the difference in temperature-related mortality with and without the UHI effect, as described in the following equation:

$$\begin{cases} M_{\text{heat\_UHI}} = \sum_{\text{mmt}}^{T_a} (M_{T_a, \text{UHI}_{\text{heat}}} - M_{T_a}) \\ M_{\text{cold\_UHI}} = \sum_{T_a}^{\text{mmt}} (M_{T_a, \text{UHI}_{\text{cold}}} - M_{T_a}) \end{cases} \quad (1)$$

where  $T_a$  represents the daily mean temperature; mmt is the MMT;  $\text{UHI}_{\text{heat}}$  and  $\text{UHI}_{\text{cold}}$  denote the UHI intensity for the warm and cold seasons, respectively;  $M_{T_a, \text{UHI}_{\text{heat}}}$  and  $M_{T_a, \text{UHI}_{\text{cold}}}$  represent the heat- and cold-related mortality with the UHI effect;  $M_{T_a}$  represents the temperature-related mortality without the UHI effect; and  $M_{\text{heat\_UHI}}$  and  $M_{\text{cold\_UHI}}$  denote the additional impacts of the UHI effect on heat- and cold-related mortality, respectively. The UHI-induced annual net impact encompassing both heat and cold-related mortality is calculated as follows:

$$M_{\text{net\_UHI}} = M_{\text{heat\_UHI}} + M_{\text{cold\_UHI}} \quad (2)$$

where  $M_{\text{net\_UHI}}$  denotes the UHI-induced annual net impact on mortality (in percentage). Positive values of  $M_{\text{heat\_UHI}}$ ,  $M_{\text{cold\_UHI}}$  and  $M_{\text{net\_UHI}}$  indicate an increase in mortality attributable to the UHI effect, while negative values suggest the opposite.  $M_{\text{net\_UHI}}$  is the sum of UHI-increased heat-related mortality (usually positive, in percentage) and UHI-reduced cold-related mortality (usually negative, in percentage).

In addition to the air temperature index, we have integrated the simplified wet bulb globe temperature<sup>73</sup> to further probe the dual impact of the UHI effect on temperature-related mortality across global cities (Supplementary Note 8). Concurrently, we further evaluated the impact of the UHI effect using the air temperature data from meteorological stations<sup>74</sup> (Supplementary Note 9). These supplementary analyses have been conducted to enhance the robustness of our conclusions.

### Assessing effects of urban cooling strategies on temperature-related mortality

We investigated the effects of two common urban cooling strategies: increasing vegetation and changing surface albedo. We examined temperature-related mortality in cities worldwide for the present (for the year 2018) and future (for the year 2050). First, we quantified the cooling effects of specific vegetation and albedo changes by analysing their relationships with urban temperatures. Next, we assessed the annual net impacts of these cooling strategies on mortality for the present and future under a moderate emissions pathway (SSP2-4.5). The detailed procedures are provided in Supplementary Fig. 13.

**Evaluating impacts of cooling strategies on temperature-related mortality for the present.** The efficacy of cooling strategies, such as increasing vegetation fraction and surface albedo, in mitigating urban temperatures can typically be assessed using numerical models such as the Weather Research and Forecasting Model<sup>75–77</sup>. However, applying such models comprehensively to more than 3,000 cities worldwide presents major challenges. Studies at global or regional scales often use remote sensing data and linear regression to evaluate the cooling impacts<sup>31,41,78</sup>. These models establish a linear relationship between temperature and vegetation, enabling statistical analysis of how vegetation changes impact temperature.

Here we applied a similar statistical method to evaluate the efficiency of cooling strategies for over 3,000 cities worldwide, following three steps. First, to incorporate temporal variation in the vegetation/albedo, we analysed the monthly linear relationships between urban temperature and vegetation/albedo for each city, separately obtaining monthly values of the fitted slopes. These slopes were used to determine the temperature changes due to vegetation and albedo

adjustments<sup>31,79</sup>. Second, we removed any anomalous slope values<sup>31</sup> that could be attributed to statistical instability or insignificance, often due to inadequate pixel data in certain cities. Finally, we utilized a random forest algorithm to establish a correction between the remaining slope values and various climatic and socioeconomic factors for both cold and warm seasons. The detailed analytical procedures are documented in Supplementary Note 11. This step allows us to determine the cooling or heating efficiency of vegetation and albedo changes by enhancing statistical stability across cities globally. The variables incorporated in the correction process include SAT, dew point temperature, precipitation, wind speed, radiation, average vegetation cover (EVI), albedo, urban population, altitude and latitude/longitude<sup>80</sup> (Supplementary Note 10). Our comprehensive assessment shows the satisfactory performance of the correction model (Supplementary Note 11).

Following previous studies<sup>81,82</sup>, we considered the use of percentage increases in vegetation and albedo as urban cooling strategies. The monthly vegetation and albedo data were averaged for both cold and warm seasons across global cities, and percentage increases were applied to the original intensity of the cold and warm seasons. To account for varying vegetation growth potential across cities with different population densities, we first classified global cities into three categories: low (0–25%), medium (25–75%) and high (75–100%) population density percentiles. High-density cities generally have lower potential for vegetation increase, and vice versa. Therefore, we applied three-tiered vegetation increase rates of 40%, 30% and 20% for low, medium, and high-density cities, respectively<sup>31,81,82</sup>. Similarly, for the albedo strategy, global cities were classified into low (0–25%), medium (25–75%) and high (75–100%) intensity classes based on albedo percentiles, and an increase of 40%, 30% and 20% was applied as the albedo regulation strategy to each class, respectively. Subsequently, we evaluated the urban cooling (UC) effects of these two strategies for individual cities (Supplementary Fig. 6). Similar to equations (1) and (2), the annual net mortality impacts ( $M_{\text{net\_UC}}$ ) attributable to increased vegetation or albedo were calculated by comparing mortality estimates with and without considering the cooling effects of these two strategies, using the following equation:

$$\left\{ \begin{array}{l} M_{\text{heat\_UC}} = \sum_{mmt}^{T_a} (M_{T_a, \text{UHI}_{\text{heat\_UC}}} - M_{T_a, \text{UHI}_{\text{heat}}}) \\ M_{\text{cold\_UC}} = \sum_{T_a}^{mmt} (M_{T_a, \text{UHI}_{\text{cold\_UC}}} - M_{T_a, \text{UHI}_{\text{cold}}}) \\ M_{\text{net\_UC}} = M_{\text{heat\_UC}} + M_{\text{cold\_UC}} \end{array} \right. \quad (3)$$

where  $M_{\text{heat\_UC}}$ ,  $M_{\text{cold\_UC}}$  and  $M_{\text{net\_UC}}$  denote the impacts of the implemented cooling strategies on heat-related, cold-related and annual net mortality, respectively, with a positive value indicating increased mortality associated with the cooling strategy and a negative value indicating decreased mortality;  $M_{T_a, \text{UHI}_{\text{heat\_UC}}}$  and  $M_{T_a, \text{UHI}_{\text{heat}}}$  represent the estimated heat-related mortality with and without the cooling effects, respectively; and  $M_{T_a, \text{UHI}_{\text{cold\_UC}}}$  and  $M_{T_a, \text{UHI}_{\text{cold}}}$  refer to the estimated cold-related mortality with and without the cooling effects, respectively.

**Evaluating impacts of cooling strategies on temperature-related mortality for the future.** The key to evaluating the impacts of cooling strategies in the future lies in estimating future urban temperatures. To address this, we follow three steps. First, we trained a random forest model to estimate UHI intensity based on a series of previously confirmed regulators including SAT, humidity, precipitation, population, and latitude/longitude<sup>37,83–85</sup> (Supplementary Note 10). Our model, validated with a randomly split 30%-test dataset, demonstrates robust accuracy with a mean correlation of 0.93 and mean absolute error of 0.18 °C (Supplementary Fig. 14). Second, with the well-validated model, we projected future UHI intensity (-2050) for each city based

on the above-mentioned predictors (Supplementary Fig. 15). Finally, we estimated future urban temperature by combining the projected future UHI intensity with the background temperature.

We designed five scenarios for vegetation and albedo strategies, varying from mild to extreme controls, to evaluate their impacts on future mortality<sup>86,87</sup>. Specifically, we set intervals of 8%, 6% and 4% for cities with low (8–40%), medium (6–30%) and high (4–20%) population density and albedo intensity classes, respectively, to assess the impact changes from low to high vegetation and albedo regulation. Notably, compared with vegetation coverage, surface albedo offers higher adjustability throughout different seasons in a year<sup>29</sup>. For example, this seasonal adjustability can be achieved by choosing roofs with an albedo that changes with sun angle, by using roofs with thermochromic materials<sup>28,41,42</sup>, or by repainting roofs and pavements<sup>43</sup>. Therefore, we modified the initial cooling strategy, which used fixed albedo values, into a more flexible strategy that mitigates the negative impact of high albedo during cold days. Note that this combined albedo strategy is engineeringly practicable<sup>29,41–43</sup>, at least over crucial areas of high vulnerability at the local scale. In this modified strategy, surface albedo was increased with different intensity strategies during warm seasons, and decreased by 8%, 6% and 4% of the initial value for cities with low, medium, and high albedo intensity classes, respectively, during cold seasons. We subsequently quantified the cooling effects of these control strategies (Supplementary Fig. 16) and examined their annual net impacts on future mortality using equation (3).

For these hypothetical heat mitigation scenarios, we quantified the impacts of the UHI effect and the associated cooling strategies on temperature-related mortality in the examined 3,000-plus cities worldwide. The impacts of the UHI effect and cooling strategies at global, climate zone, continental and individual city scales were comprehensively revealed separately (Figs. 2 and 3, and Supplementary Fig. 9). We acknowledge uncertainties in the analysis, such as the omission of vegetation type and distinct weather conditions (for example, snowfall). Additionally, the  $M-T$  association might change in the future. Nevertheless, these uncertainties would not undermine our key findings, even if some of the magnitudes of the effects are shifted. Further deliberation on these uncertainties can be found in Supplementary Note 12.

## Reporting summary

Further information on research design is available in the Nature Portfolio Reporting Summary linked to this article.

## Data availability

All the satellite and reanalysis data used in this study can be downloaded on the Google Earth Engine platform (<https://developers.google.cn/earth-engine/datasets/catalog/>). Global climate simulations for future periods are available at <https://esgf-node.llnl.gov/search/cmip6/>. The global 1 km near-surface air temperature dataset is available at <https://doi.org/10.25380/iastate.c.6005185.v1>. The GDP and population data are available via Figshare at <https://doi.org/10.6084/m9.figshare.17004523.v1> (ref. 88) and <https://landscan.ornl.gov/>, respectively. The GUB dataset is available at <https://data-starcloudpcl.ac.cn/>. The Köppen–Geiger climate zone dataset is available at <https://koeppen-geiger.vu-wien.ac.at/>. The global vector boundary base map is available at <https://gadm.org/>. The generated datasets of this study are publicly available at <https://github.com/Wangshasha929/urban-heat.git>.

## Code availability

The Google Earth Engine platform (<https://code.earthengine.google.com/>), Python (version 3.8) and MATLAB (version R2018a) were primarily employed for analysis. The primary analysis code is publicly available at <https://github.com/Wangshasha929/urban-heat.git> and via Zenodo at <https://doi.org/10.5281/zenodo.14869462> (ref. 89).

## References

47. Li, X. et al. Mapping global urban boundaries from the global artificial impervious area (GAIA) data. *Environ. Res. Lett.* **15**, 094044 (2020).
48. Kottek, M., Grieser, J., Beck, C., Rudolf, B. & Rubel, F. World map of the Koppen–Geiger climate classification updated. *Meteorol. Z.* **15**, 259–263 (2006).
49. Zhang, T. et al. A global dataset of daily near-surface air temperature at 1 km resolution over land (2003–2020). *Earth Syst. Sci. Data* **14**, 5637–5649 (2022).
50. Gatti, P. L. *Probability Theory and Mathematical Statistics for Engineers* (CRC Press, 2004).
51. Eyring, V. et al. Overview of the Coupled Model Intercomparison Project Phase 6 (CMIP6) experimental design and organization. *Geosci. Model Dev.* **9**, 1937–1958 (2016).
52. O'Neill, B. C. et al. The Scenario Model Intercomparison Project (ScenarioMIP) for CMIP6. *Geosci. Model Dev.* **9**, 3461–3482 (2016).
53. Muñoz-Sabater, J. et al. ERA5-Land: a state-of-the-art global reanalysis dataset for land applications. *Earth Syst. Sci. Data* **13**, 4349–4383 (2021).
54. Chen, J. et al. Global 1km × 1km gridded revised real gross domestic product and electricity consumption during 1992–2019 based on calibrated nighttime light data. *Sci. Data* **9**, 202 (2022).
55. Nirandjan, S., Koks, E. E., Ward, P. J. & Aerts, J. C. A spatially-explicit harmonized global dataset of critical infrastructure. *Sci. Data* **9**, 150 (2022).
56. Kummu, M., Taka, M. & Guillaume, J. H. Gridded global datasets for gross domestic product and Human Development Index over 1990–2015. *Sci. Data* **5**, 180004 (2018).
57. Dobson, J. E. LandScan: a global population database for estimating populations at risk. *Photogramm. Eng. Remote Sens.* **66**, 849–857 (2000).
58. Gao, J. *Downscaling Global Spatial Population Projections from 1/8-degree to 1-km Grid Cells* (National Center for Atmospheric Research, 2017).
59. Krummenauer, L. et al. Global drivers of minimum mortality temperatures in cities. *Sci. Total Environ.* **695**, 133560 (2019).
60. Gesch, D. B., Verdin, K. L. & Greenlee, S. K. New land surface digital elevation model covers the Earth. *Eos* **80**, 69–70 (1999).
61. Menashe, D. S. & Friedl, M. A. *User Guide to Collection 6 MODIS Land Cover (MCD12Q1 and MCD12C1) Product* (USGS, 2018); [https://lpdaac.usgs.gov/documents/101/MCD12\\_User\\_Guide\\_V6.pdf](https://lpdaac.usgs.gov/documents/101/MCD12_User_Guide_V6.pdf)
62. Gasparrini, A. et al. Small-area assessment of temperature-related mortality risks in England and Wales: a case time series analysis. *Lancet Planet. Health* **6**, e557–e564 (2022).
63. Achebak, H., Devolder, D., Ingole, V. & Ballester, B. Reversal of the seasonality of temperature-attributable mortality from respiratory diseases in Spain. *Nat. Commun.* **11**, 2457 (2020).
64. Huber, V. et al. Temperature-related excess mortality in German cities at 2°C and higher degrees of global warming. *Environ. Res.* **186**, 109447 (2020).
65. Lee, W. H. et al. An investigation on attributes of ambient temperature and diurnal temperature range on mortality in five East-Asian countries. *Sci. Rep.* **7**, 10207 (2017).
66. Madanian, M. et al. The study of thermal pattern changes using Landsat-derived land surface temperature in the central part of Isfahan province. *Sustain. Cities Soc.* **39**, 650–661 (2018).
67. Peng, S. et al. Surface urban heat island across 419 global big cities. *Environ. Sci. Technol.* **46**, 696–703 (2012).
68. Imhoff, M. L., Zhang, P., Wolfe, E. R. & Bounoua, L. Remote sensing of the urban heat island effect across biomes in the continental USA. *Remote Sens. Environ.* **114**, 504–513 (2010).
69. Yao, R., Wang, L., Huang, X., Gong, W. & Xia, X. Greening in rural areas increases the surface urban heat island intensity. *Geophys. Res. Lett.* **46**, 2204–2212 (2019).
70. Anderson, B. G. & Bell, M. L. Weather-related mortality: how heat, cold, and heat waves affect mortality in the United States. *Epidemiology* **20**, 205–213 (2009).
71. Guo, Y. et al. Global variation in the effects of ambient temperature on mortality: a systematic evaluation. *Epidemiology* **25**, 781–789 (2014).
72. Yin, Q., Wang, J., Ren, Z., Li, J. & Guo, Y. Mapping the increased minimum mortality temperatures in the context of global climate change. *Nat. Commun.* **10**, 4640 (2019).
73. Buzan, J. R., Oleson, K. & Huber, M. Implementation and comparison of a suite of heat stress metrics within the Community Land Model version 4.5. *Geosci. Model Dev.* **8**, 151–170 (2015).
74. Rohde, R. et al. Berkeley Earth temperature averaging process. *Geoinform. Geostatist. Overview* **1**, 20–100 (2013).
75. Tewari, M. et al. Interaction of urban heat islands and heat waves under current and future climate conditions and their mitigation using green and cool roofs in New York City and Phoenix, Arizona. *Environ. Res. Lett.* **14**, 034002 (2019).
76. Synnefa, A., Dandou, A., Santamouris, M., Tombrou, M. & Soulakellis, N. On the use of cool materials as a heat island mitigation strategy. *J. Appl. Meteorol. Clim.* **47**, 2846–2856 (2008).
77. Zinzi, M. & Agnoli, S. Cool and green roofs. An energy and comfort comparison between passive cooling and mitigation urban heat island techniques for residential buildings in the Mediterranean region. *Energy Build.* **55**, 66–76 (2012).
78. Wang, J. et al. Significant effects of ecological context on urban trees' cooling efficiency. *ISPRS J. Photogramm. Remote Sens.* **159**, 78–89 (2020).
79. Marando, F. et al. Urban heat island mitigation by green infrastructure in European functional urban areas. *Sustain. Cities Soc.* **77**, 103564 (2022).
80. Schwaab, J. et al. The role of urban trees in reducing land surface temperatures in European cities. *Nat. Commun.* **12**, 6763 (2021).
81. Lobaccaro, G. & Aceri, J. A. Comparative analysis of green actions to improve outdoor thermal comfort inside typical urban street canyons. *Urban Clim.* **14**, 251–267 (2015).
82. Jandaghian, Z. & Akbari, H. Increasing urban albedo to reduce heat-related mortality in Toronto and Montreal, Canada. *Energy Build.* **237**, 110697 (2021).
83. Manoli, G. et al. Magnitude of urban heat islands largely explained by climate and population. *Nature* **573**, 55–60 (2019).
84. Venter, Z. S., Chakraborty, T. & Lee, X. Crowdsourced air temperatures contrast satellite measures of the urban heat island and its mechanisms. *Sci. Adv.* **7**, eabb9569 (2021).
85. Zhao, L., Lee, X., Smith, B. R. & Oleson, K. Strong contributions of local background climate to urban heat islands. *Nature* **511**, 216–219 (2014).
86. Jacobson, M. Z. & Hoeve, J. E. T. Effects of urban surfaces and white roofs on global and regional climate. *J. Clim.* **25**, 1028–1044 (2012).
87. Virk, G. et al. Microclimatic effects of green and cool roofs in London and their impacts on energy use for a typical office building. *Energy Build.* **88**, 214–228 (2015).
88. Chen, J. & Gao, M. Global 1 km × 1 km gridded revised real gross domestic product and electricity consumption during 1992–2019 based on calibrated nighttime light data. *Figshare* <https://doi.org/10.6084/m9.figshare.17004523.v1> (2021).
89. Wang, S. et al. Wangshasha929/urban-heat: dual impact of global urban overheating on mortality. *Zenodo* <https://doi.org/10.5281/zenodo.14869462> (2025).

## Acknowledgements

Our study was supported by the National Natural Science Foundation of China (grant no. 42171306) and the Fundamental Research Funds for the Central Universities (grant 2024300388). We also acknowledge the support from the National Youth Talent Support Program of China. T.C.'s contribution was supported by the US Department of Energy (DOE), Office of Science, Biological and Environmental Research Program, through the Early Career Research Program. Pacific Northwest National Laboratory is operated for the DOE by Battelle Memorial Institute under contract DE-AC05-76RL01830. We thank J. L. Kephart of Drexel University for valuable insights and discussions.

## Author contributions

W.Z. designed the research; S.W. and W.Z. performed the data analysis; S.W. and W.Z. wrote the manuscript; and B.Z., S.T., T.C., Z.W., K.H., H.D., A.M., J.L., Z.L., L.L., F.H. and M.L. contributed ideas to the data analysis, interpretation of results or manuscript revisions.

## Competing interests

The authors declare no competing interests.

## Additional information

**Supplementary information** The online version contains supplementary material available at <https://doi.org/10.1038/s41558-025-02303-3>.

**Correspondence and requests for materials** should be addressed to Wenfeng Zhan.

**Peer review information** *Nature Climate Change* thanks Yifan Fan, Emanuele Massaro and the other, anonymous, reviewer(s) for their contribution to the peer review of this work.

**Reprints and permissions information** is available at [www.nature.com/reprints](http://www.nature.com/reprints).

## Reporting Summary

Nature Portfolio wishes to improve the reproducibility of the work that we publish. This form provides structure for consistency and transparency in reporting. For further information on Nature Portfolio policies, see our [Editorial Policies](#) and the [Editorial Policy Checklist](#).

### Statistics

For all statistical analyses, confirm that the following items are present in the figure legend, table legend, main text, or Methods section.

n/a Confirmed

- The exact sample size ( $n$ ) for each experimental group/condition, given as a discrete number and unit of measurement
- A statement on whether measurements were taken from distinct samples or whether the same sample was measured repeatedly
- The statistical test(s) used AND whether they are one- or two-sided  
*Only common tests should be described solely by name; describe more complex techniques in the Methods section.*
- A description of all covariates tested
- A description of any assumptions or corrections, such as tests of normality and adjustment for multiple comparisons
- A full description of the statistical parameters including central tendency (e.g. means) or other basic estimates (e.g. regression coefficient) AND variation (e.g. standard deviation) or associated estimates of uncertainty (e.g. confidence intervals)
- For null hypothesis testing, the test statistic (e.g.  $F$ ,  $t$ ,  $r$ ) with confidence intervals, effect sizes, degrees of freedom and  $P$  value noted  
*Give P values as exact values whenever suitable.*
- For Bayesian analysis, information on the choice of priors and Markov chain Monte Carlo settings
- For hierarchical and complex designs, identification of the appropriate level for tests and full reporting of outcomes
- Estimates of effect sizes (e.g. Cohen's  $d$ , Pearson's  $r$ ), indicating how they were calculated

*Our web collection on [statistics for biologists](#) contains articles on many of the points above.*

### Software and code

Policy information about [availability of computer code](#)

Data collection All the datasets used in this study are publicly accessible and no software was used.

Data analysis Python 3.8 was used for data analysis, which was compiled in PyCharm 2020.3. In addition, Google Earth Engine and Matlab R 2018a were also employed for data analysis in this study.

For manuscripts utilizing custom algorithms or software that are central to the research but not yet described in published literature, software must be made available to editors and reviewers. We strongly encourage code deposition in a community repository (e.g. GitHub). See the Nature Portfolio [guidelines for submitting code & software](#) for further information.

### Data

Policy information about [availability of data](#)

All manuscripts must include a [data availability statement](#). This statement should provide the following information, where applicable:

- Accession codes, unique identifiers, or web links for publicly available datasets
- A description of any restrictions on data availability
- For clinical datasets or third party data, please ensure that the statement adheres to our [policy](#)

All the datasets used in this study are publicly accessible. All the satellite and reanalysis data used in this study can be downloaded on the Google Earth Engine (GEE) platform (<https://developers.google.cn/earth-engine/datasets/catalog/>). Global climate simulations for future periods are available at <https://esgf-node.llnl.gov/search/cmip6/>. The global 1 km near-surface air temperature dataset are available at <https://doi.org/10.25380/iastate.c.6005185.v1>. The Gross

Domestic Product (GDP) and population data are available at <https://doi.org/10.6084/m9.figshare.17004523.v1> and <https://landscan.ornl.gov/>, respectively. The global urban boundary dataset is available at <http://data.ess.tsinghua.edu.cn/>. The generated datasets of this study are publicly available at <https://github.com/Wangshasha929/urban-heat.git>.

## Human research participants

Policy information about [studies involving human research participants and Sex and Gender in Research](#).

Reporting on sex and gender	<input type="checkbox"/> Sex and gender were not considered in this study.
Population characteristics	Human research participants were not involved in this study.
Recruitment	None.
Ethics oversight	None.

Note that full information on the approval of the study protocol must also be provided in the manuscript.

## Field-specific reporting

Please select the one below that is the best fit for your research. If you are not sure, read the appropriate sections before making your selection.

Life sciences       Behavioural & social sciences       Ecological, evolutionary & environmental sciences

For a reference copy of the document with all sections, see [nature.com/documents/nr-reporting-summary-flat.pdf](https://nature.com/documents/nr-reporting-summary-flat.pdf)

## Ecological, evolutionary & environmental sciences study design

All studies must disclose on these points even when the disclosure is negative.

Study description	We examine the beneficial and detrimental effects of the urban heat islands (UHI) and associated cooling interventions (including both increased urban vegetation and albedo modifications) on mortality in over 3,000 cities worldwide. Data including multi-source remote sensing, climate data, and empirically derived mortality-temperature associations are used for analysis.
Research sample	We chose 3,280 cities worldwide to investigate the impacts of the UHI and urban cooling strategies on annual net temperature-related mortality. These cities span across equatorial (441 cities), arid (379 cities), warm (1706 cities), and snow cities (754 cities). The MODIS data consist of the 16-day enhanced vegetation index (EVI; product name: MOD13Q1; 250 m spatial resolution) and the daily albedo estimates (MCD43A3; 500 m). The urban air temperature data were obtained from the global near-surface air temperature dataset (1 km spatial resolution; <a href="https://doi.org/10.25380/iastate.c.6005185.v1">https://doi.org/10.25380/iastate.c.6005185.v1</a> ). The climate were obtained from the ERA5-Daily and monthly ERA5-Land reanalysis datasets and the Coupled Model Intercomparison Project Phase 6 (CMIP6). GDP data were extracted from the global long-term GDP dataset (1 km spatial resolution; <a href="https://doi.org/10.6084/m9.figshare.17004523.v1">https://doi.org/10.6084/m9.figshare.17004523.v1</a> ). Historical population data were obtained from the Oak Ridge National Laboratory's LandScan population dataset ( <a href="https://landscan.ornl.gov/">https://landscan.ornl.gov/</a> ). Population data in various countries and territories were also obtained from the United Nations. The elevation data were derived from the GTOPO30 dataset (1 km) provided by the U.S. Geological Survey's Center for Earth Resources Observation and Science ( <a href="http://lpdaac.usgs.gov">http://lpdaac.usgs.gov</a> ). The land cover type data were sourced from the MODIS MCD12Q1 product (500 m spatial resolution).
Sampling strategy	We chose cities with an urban area greater than 30 square kilometers in 2018 across the globe and obtained 3280 cities in total worldwide. We consider this is adequate to represent global major urban population as every single city that satisfies this sampling criterion has been selected.
Data collection	All the satellite and reanalysis data used in this study can be downloaded on the Google Earth Engine (GEE) platform ( <a href="https://developers.google.cn/earth-engine/datasets/catalog/">https://developers.google.cn/earth-engine/datasets/catalog/</a> ). Global climate simulations for future periods are available at <a href="https://esgf-node.llnl.gov/search/cmip6/">https://esgf-node.llnl.gov/search/cmip6/</a> . The global 1 km near-surface air temperature dataset are available at <a href="https://doi.org/10.25380/iastate.c.6005185.v1">https://doi.org/10.25380/iastate.c.6005185.v1</a> . The Gross Domestic Product (GDP) and population data are available at <a href="https://doi.org/10.6084/m9.figshare.17004523.v1">https://doi.org/10.6084/m9.figshare.17004523.v1</a> and <a href="https://landscan.ornl.gov/">https://landscan.ornl.gov/</a> , respectively. The global urban boundary dataset is available at <a href="http://data.ess.tsinghua.edu.cn/">http://data.ess.tsinghua.edu.cn/</a> .
Timing and spatial scale	Our study was conducted at two time-scales: daily and annual. The daily data (e.g., climate data) were used to derive the daily air temperature and the cumulative heat and cold-related mortality. The annual analysis were performed to assess the net impacts of the UHI and urban cooling strategies on temperature-related mortality. In terms of spatial scale, our study was conducted for every single city across the chosen 3280 cities worldwide.
Data exclusions	No data were excluded from the analysis.
Reproducibility	All attempts to repeat the experiment were successful.
Randomization	The chosen 3280 cities worldwide were allocated by continent and climate zone. This allocation strategy is very common and well

Randomization

accepted in urban studies across the globe.

Blinding

Blinding is not relevant to our study because no recruitment of participant is necessary for our study.

Did the study involve field work?  Yes  No

## Reporting for specific materials, systems and methods

We require information from authors about some types of materials, experimental systems and methods used in many studies. Here, indicate whether each material, system or method listed is relevant to your study. If you are not sure if a list item applies to your research, read the appropriate section before selecting a response.

### Materials & experimental systems

n/a	Involved in the study
<input checked="" type="checkbox"/>	<input type="checkbox"/> Antibodies
<input checked="" type="checkbox"/>	<input type="checkbox"/> Eukaryotic cell lines
<input checked="" type="checkbox"/>	<input type="checkbox"/> Palaeontology and archaeology
<input checked="" type="checkbox"/>	<input type="checkbox"/> Animals and other organisms
<input checked="" type="checkbox"/>	<input type="checkbox"/> Clinical data
<input checked="" type="checkbox"/>	<input type="checkbox"/> Dual use research of concern

### Methods

n/a	Involved in the study
<input checked="" type="checkbox"/>	<input type="checkbox"/> ChIP-seq
<input checked="" type="checkbox"/>	<input type="checkbox"/> Flow cytometry
<input checked="" type="checkbox"/>	<input type="checkbox"/> MRI-based neuroimaging

## Terms and Conditions

Springer Nature journal content, brought to you courtesy of Springer Nature Customer Service Center GmbH (“Springer Nature”). Springer Nature supports a reasonable amount of sharing of research papers by authors, subscribers and authorised users (“Users”), for small-scale personal, non-commercial use provided that all copyright, trade and service marks and other proprietary notices are maintained. By accessing, sharing, receiving or otherwise using the Springer Nature journal content you agree to these terms of use (“Terms”). For these purposes, Springer Nature considers academic use (by researchers and students) to be non-commercial.

These Terms are supplementary and will apply in addition to any applicable website terms and conditions, a relevant site licence or a personal subscription. These Terms will prevail over any conflict or ambiguity with regards to the relevant terms, a site licence or a personal subscription (to the extent of the conflict or ambiguity only). For Creative Commons-licensed articles, the terms of the Creative Commons license used will apply.

We collect and use personal data to provide access to the Springer Nature journal content. We may also use these personal data internally within ResearchGate and Springer Nature and as agreed share it, in an anonymised way, for purposes of tracking, analysis and reporting. We will not otherwise disclose your personal data outside the ResearchGate or the Springer Nature group of companies unless we have your permission as detailed in the Privacy Policy.

While Users may use the Springer Nature journal content for small scale, personal non-commercial use, it is important to note that Users may not:

1. use such content for the purpose of providing other users with access on a regular or large scale basis or as a means to circumvent access control;
2. use such content where to do so would be considered a criminal or statutory offence in any jurisdiction, or gives rise to civil liability, or is otherwise unlawful;
3. falsely or misleadingly imply or suggest endorsement, approval , sponsorship, or association unless explicitly agreed to by Springer Nature in writing;
4. use bots or other automated methods to access the content or redirect messages
5. override any security feature or exclusionary protocol; or
6. share the content in order to create substitute for Springer Nature products or services or a systematic database of Springer Nature journal content.

In line with the restriction against commercial use, Springer Nature does not permit the creation of a product or service that creates revenue, royalties, rent or income from our content or its inclusion as part of a paid for service or for other commercial gain. Springer Nature journal content cannot be used for inter-library loans and librarians may not upload Springer Nature journal content on a large scale into their, or any other, institutional repository.

These terms of use are reviewed regularly and may be amended at any time. Springer Nature is not obligated to publish any information or content on this website and may remove it or features or functionality at our sole discretion, at any time with or without notice. Springer Nature may revoke this licence to you at any time and remove access to any copies of the Springer Nature journal content which have been saved.

To the fullest extent permitted by law, Springer Nature makes no warranties, representations or guarantees to Users, either express or implied with respect to the Springer nature journal content and all parties disclaim and waive any implied warranties or warranties imposed by law, including merchantability or fitness for any particular purpose.

Please note that these rights do not automatically extend to content, data or other material published by Springer Nature that may be licensed from third parties.

If you would like to use or distribute our Springer Nature journal content to a wider audience or on a regular basis or in any other manner not expressly permitted by these Terms, please contact Springer Nature at

[onlineservice@springernature.com](mailto:onlineservice@springernature.com)